

Article

# Alkaline Earth Element Adsorption onto PAA-Coated Magnetic Nanoparticles

Qing Wang <sup>1</sup>, Valentina Prigiobbe <sup>2,\*</sup>, Chun Huh <sup>3</sup> and Steven L. Bryant <sup>4</sup>

<sup>1</sup> Department of Chemical and Biomolecular Engineering, Rice University, Houston, TX 77005, USA; wangqing1230@gmail.com

<sup>2</sup> Department of Civil, Environmental, and Ocean Engineering, Stevens Institute of Technology, Hoboken, NJ 07030, USA

<sup>3</sup> Department of Petroleum and Geosystems Engineering, The University of Texas at Austin, Austin, TX 78712, USA; chunhuh@mail.utexas.edu

<sup>4</sup> Department of Chemical and Petroleum Engineering, University of Calgary, Calgary, AB T2N 1N4, Canada; steven.bryant@ucalgary.ca

\* Correspondence: valentina.prigiobbe@stevens.edu Tel.: +1-201-216-5310

Academic Editor: Dongsheng Wen

Received: 3 January 2017; Accepted: 8 February 2017; Published: 14 February 2017

**Abstract:** In this paper, we present a study on the adsorption of calcium ( $\text{Ca}^{2+}$ ) onto polyacrylic acid-functionalized iron-oxide magnetic nanoparticles (PAA-MNPs) to gain an insight into the adsorption behavior of alkaline earth elements at conditions typical of produced water from hydraulic fracturing. An aqueous co-precipitation method was employed to fabricate iron oxide magnetic nanoparticles, whose surface was first coated with amine and then by PAA. To evaluate the  $\text{Ca}^{2+}$  adsorption capacity by PAA-MNPs, the  $\text{Ca}^{2+}$  adsorption isotherm was measured in batch as a function of pH and sodium chlorite (electrolyte) concentration. A surface complexation model accounting for the coulombic forces in the diffuse double layer was developed to describe the competitive adsorption of protons ( $\text{H}^+$ ) and  $\text{Ca}^{2+}$  onto the anionic carboxyl ligands of the PAA-MNPs. Measurements show that  $\text{Ca}^{2+}$  adsorption is significant above pH 5 and decreases with the electrolyte concentration. Upon adsorption, the nanoparticle suspension destabilizes and creates large clusters, which favor an efficient magnetic separation of the PAA-MNPs, therefore, helping their recovery and recycle. The model agrees well with the experiments and predicts that the maximum adsorption capacity can be achieved within the pH range of the produced water, although that maximum declines with the electrolyte concentration.

**Keywords:** adsorption; calcium; functionalized superparamagnetic iron oxide nanoparticles; polyacrylic acid; surface complexation modelling

## 1. Introduction

Produced water generated during the production of unconventional gas from onshore activities is, on average, 600 million  $\text{m}^3$  per year [1,2]. Significant costs are involved in purchasing fresh water, transporting it to the site, and transporting the produced water to treatment and disposal locations. Therefore, the management and disposal of this water has emerged as a central concern in the development of fracking [3]. The salinity of the produced water can be as high as four times the salinity of the seawater and values up to nine times have also been observed [4]. Calcium ( $\text{Ca}^{2+}$ ), barium ( $\text{Ba}^{2+}$ ), sodium ( $\text{Na}^+$ ), strontium ( $\text{Sr}^{2+}$ ), and radium ( $\text{Ra}^{2+}$  as isotopes  $^{226}\text{Ra}$  and  $^{228}\text{Ra}$ ) are among the cations and the radionuclides with the largest concentration. They exceed the standards for reuse in agriculture or discharge into water bodies issued by state agencies through National Pollutant Discharge Elimination System (NPDES) permits. Recently, the external reuse of the produced water is

becoming an attractive alternative to the current practice [5]. However, produced water for external reuse requires desalination and current techniques face significant engineering challenges because of the large volume, hyper-salinity, and complicated composition of the water. Results show that crystallization is a feasible process for the removal of the major metal cations in the produced water, but due to the low supersaturation ratios precipitation of co-crystals might be favored [2]. Therefore, it would be envisaged to create a concentrated supersaturated brine of selected cations to allow fast precipitation of homogenous crystals.

Nano-scale adsorbents are considered as an ideal candidate for the removal of selected ions because of their large surface area per mass and a great number of selectively active sites that can be generated on the surface. Among these nano-adsorbents, the iron-oxide based magnetic nanoparticles have been extensively investigated to remove multi-valent cations, such as copper, lead, zinc, nickel [6–8], as they have a number of advantages, including easy control, fast separation of the spent nanoparticles from the cleaned water with the application of magnetic field gradient, and the potential for the spent nanoparticles to be regenerated and reused. However, their ion selectivity and adsorption capacity reported to date are unsatisfactory [7,9–12]. With the aim to improve the adsorption capacity and ion selectivity, and the nanoparticle dispersion stability, the iron-oxide magnetic nanoparticles are conjugated on the surface with functional groups like carboxylate, hydroxyl and amino groups which have high affinity for cations to form metal complexes or chelates [13–15]. Selecting an appropriate functional material to modify the iron-oxide nanoparticles is of great importance in developing a high-performance magnetic nano-adsorbent. Polyacrylic acid (PAA) is used as an emulsifier and thickening agent for aqueous solutions and dispersions. In the recent years, it has been employed to make polymer-based hybrid adsorbents to effectively remove organic and inorganic pollutants [16,17]. Recently, several authors have studied the use of PAA and modified-PAA to remove heavy metals, such as cadmium, chromium, copper, lead, mercury, nickel, and zinc [18–20] from waste water. In all cases, high removal efficiency under broad interval of pH and temperature has been observed. However, few studies have been dedicated to the adsorption of alkaline earth elements onto PAA [21,22]. The work by Bartós and Bilewicz [22] shows significant adsorption of  $Ba^{2+}$ ,  $Ra^{2+}$ , and  $Sr^{2+}$  by PAA, but the effect of pH and ionic strength was not investigated extensively, in particular under the conditions of interest of this work.

Here, we propose a technique to selectively separate ions from produced water and, then, create a highly supersaturated brine. It consists in using functionalized magnetic nanoparticles which can selectively adsorb targeted cations from produced water and be separated with a magnet from the treated water. They can be therefore regenerated for reuse producing a concentrated brine [12]. This paper presents the results from the study of the adsorption of  $Ca^{2+}$ , a representative alkaline earth element and a congener of  $Ba^{2+}$ ,  $Ra^{2+}$ , and  $Sr^{2+}$ , by iron-oxide magnetic nanoparticles (MNPs) functionalized with PAA. An aqueous co-precipitation method was employed to fabricate iron-oxide magnetic nanoparticles, which was followed by the surface modification with the amine group [23–26]. PAA was then conjugated on the surface of the amine-MNPs. The effect of pH and salinity on the removal of  $Ca^{2+}$  was investigated in batch experiments as a function of solution pH and electrolyte (NaCl) concentration to understand the effect of pH and salinity on adsorption. A surface complexation model accounting for the electrostatic forces was implemented to describe the competitive adsorption between protons ( $H^+$ ) and  $Ca^{2+}$  onto an anionic adsorption site available on the surface of PAA-MNPs. The model well describes the pH-dependent adsorption of  $Ca^{2+}$  onto the PAA-MNPs as a function of electrolyte concentration and it is used to make prediction on the adsorption of a general alkaline-Earth element from produced water.

The paper is divided into four sections. Section 2 reports and discusses the results of nanoparticle synthesis and characterization, of the adsorption experiments and optimization, and of the simulations of adsorption. Section 3 describes the materials and the methods used in this work, including the developed surface complexation model. Finally, Section 4 draws the conclusions.

## 2. Results and Discussion

### 2.1. Characterization of the Synthesized Nanoparticles

TEM images obtained for MNPs, NH<sub>2</sub>-MNPs, and PAA-MNPs are presented in Figure 1. According to the TEM images, the MNPs (Figure 1a) formed nanoclusters of single nanoparticles with a diameter of approximately 10 nm, which is measured by ImageJ (NIH, Bethesda, MD, USA). The majority of nanoparticles were in a polygonal shape with rough surface, which is in agreement with previous observations [27]. Coating with amine and different molecular weights of PAA, the nanoparticles have the same morphology, as shown in Figure 1b–e.

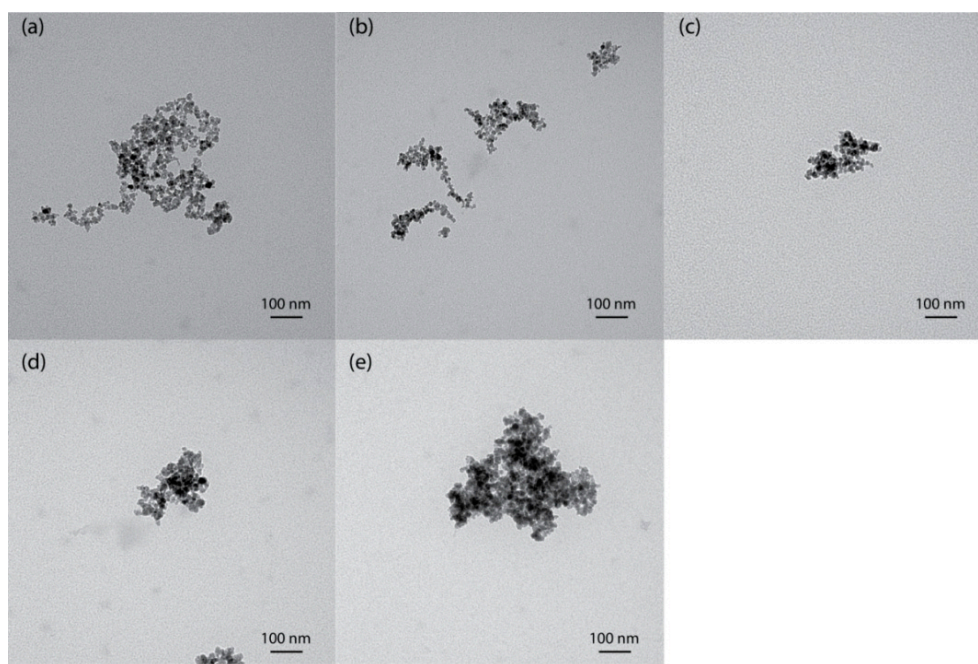


**Figure 1.** TEM images of (a) MNPs; (b) NH<sub>2</sub>-MNPs; (c) PAA-8k-MNPs; (d) PAA-100k-MNPs; and (e) PAA-450k-MNPs.

Measurements of the distribution of the hydrodynamic diameter are presented in Figure 2. Here, it is possible to notice that the average hydrodynamic diameter of MNP nanocluster is approximately  $89.5 \pm 4.4$  nm. As the amine group is added to the MNP surface, the hydrodynamic diameter increases to  $131.0 \pm 7.4$  nm. Coating nanoparticles with PAA of different molecular weight, namely, 8000, 100,000 and 450,000 dalton, the average hydrodynamic diameter of MNP nanocluster increases further to  $149.3 \pm 7.9$ ,  $204.8 \pm 9.2$ , and  $369.5 \pm 18.5$  nm, respectively. Among these five types of nanoparticles, NH<sub>2</sub>-MNP nanoclusters show a relatively narrow size distribution with the polydispersity index at 0.082. Much larger hydrodynamic diameter was observed for PAA-450k-MNP nanoclusters, the relative long chain length of polyacrylic acid as well as their ability to affect surrounding water area. This kind of interaction is present in all synthesized nanoparticles. Due to the long chain length of PAA, the nanoclusters might tangle with each other, which also contribute to the larger size of hydrodynamic diameter of MNP nanoclusters. However, the size of aggregation might depend on the ratio of the amine group on the MNPs and carboxyl groups of PAA [28]. However, in this work the number of amine group on the surface of MNPs was not adjusted to control the size. Among the synthesized types of PAA-MNPs, the nanoparticles coated with the PAA of the lowest molecular weight, i.e., PAA-8k-MNPs, showed the smallest nanoclusters (Figure 1c) and the narrowest distribution, and hence, the largest surface area available for adsorption. Therefore, PAA-8k-MNPs were selected for

the study of cation removal. Below, they are identified as PAA-MNPs for simplicity. Their measured specific surface area with the Brunauer-Emmett-Teller (BET) method was equal to  $22.9 \text{ m}^2/\text{g}$ .

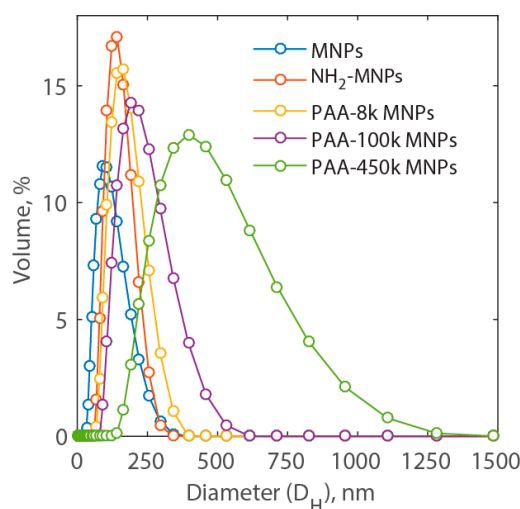


**Figure 2.** Hydrodynamic diameter ( $D_H$ ) distribution of MNPs,  $\text{NH}_2$ -MNPs, PAA-8k-MNPs, PAA-100k-MNPs, and PAA-450k-MNPs in  $\text{DI-H}_2\text{O}$ .

The measured values of the zeta potential,  $\zeta$ , were  $-18.2 \pm 0.9 \text{ mV}$ ,  $25.9 \pm 1.2 \text{ mV}$ , and  $-39.1 \pm 1.0 \text{ mV}$  for the MNPs,  $\text{NH}_2$ -MNPs, and PAA-MNPs, correspondingly. The successful functionalization of the nanoparticles with the amine group and carboxylic group was proven by zeta potential analysis, and demonstrated by the inversions of zeta potential from negative (MNPs) to positive ( $\text{NH}_2$ -MNPs) to negative (PAA-MNPs).

The mass fraction of surface coating on MNPs was reported as the percentage loss of weight and the curves are shown in Figure 3. A continuous weight loss was observed for both amine and PAA coated magnetic nanoparticles when the temperature was increased from  $50 \text{ }^\circ\text{C}$  to  $600 \text{ }^\circ\text{C}$ . The weight loss of MNPs is 5.3%, which is contributed by physically- and chemically-adsorbed water, and citric acid was used to stabilize the bare nanoparticles. The overall weight loss of the  $\text{NH}_2$ -MNPs is approximately 8.5 wt %, which includes the decomposition of the amine group and of the citric acid. The overall weight loss of the PAA-MNPs is 13.7 wt % and subtracting the weight loss due to the decomposition of the amine group and citric acid from the overall weight loss of the PAA-MNPs, the amount of PAA is 5.2 wt %.

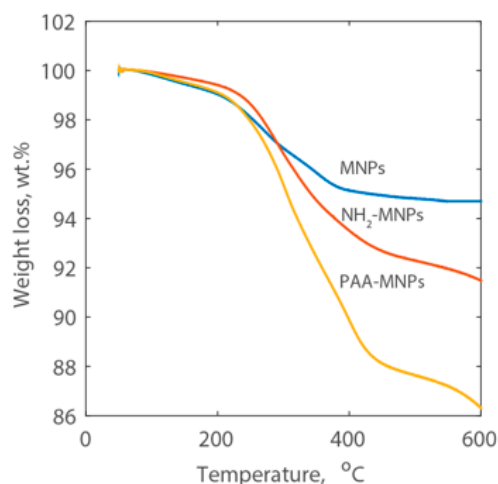


**Figure 3.** TGA curves of MNPs,  $\text{NH}_2$ -MNPs, and PAA-MNPs.

The XRD patterns of the synthesized MNPs are reported in Figure 4. They show the characteristic peaks for magnetite at  $2\theta$  corresponding to  $30.1^\circ$ ,  $35.5^\circ$ ,  $43.1^\circ$ ,  $53.4^\circ$ ,  $57.0^\circ$ , and  $62.6^\circ$  (JCPDS cards #75-0033), demonstrating that the modification of iron-oxide magnetic nanoparticles with amine group and polyacrylic acid does not result in the phase change of magnetite. The sharpness of the peaks also indicates the high crystallinity of the PAA-MNPs.

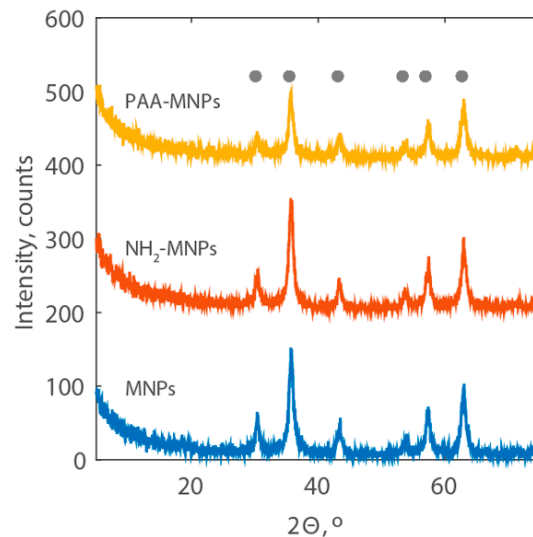


**Figure 4.** XRD patterns of MNPs,  $\text{NH}_2$ -MNPs, and PAA-MNPs with the location of the peaks of the reference magnetite (grey dots).

Figure 5 shows the Langevin curves measured by VSM for the nanoparticle liquid suspensions. The absence of hysteresis indicates that the MNPs do not retain magnetization in the absence of a magnetic field. These results, along with the high saturation magnetization (approximately 90 emu/g of MNPs) indicate that the synthesized particles are superparamagnetic. This behavior is due to the small size of the individual magnetic nanoparticles, which is approximately 10 nm [29]. The magnetization curves are very close for the MNPs and  $\text{NH}_2$ -MNPs.

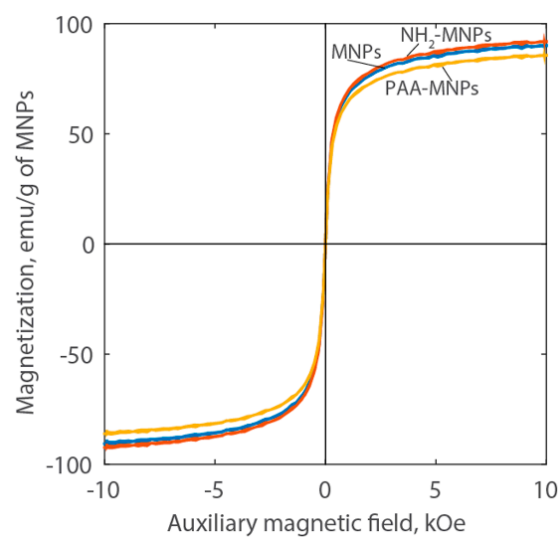


**Figure 5.** Langevin curves of MNPs,  $\text{NH}_2$ -MNPs, and PAA-MNPs at room temperature.

## 2.2. Adsorption Experiments

Preliminary tests to compare the adsorption of the cation on both bare- and PAA-MNPs were carried out. The conditions were selected within the pH range where both types of MNPs have the maximum affinity towards  $\text{Ca}^{2+}$ , i.e., pH greater than 6. The results are expressed as adsorption capacity (mol/g):

$$q_e = \frac{z_i V}{m_{\text{NP}}}, \quad (1)$$

with  $z_i$  is the adsorbed concentration of the cation on the PAA-MNP surface (mol/kg),  $V$  is the volume of the suspension ( $\text{m}^3$ ), and  $m_{\text{NP}}$  the mass of nanoparticles in suspension (g). At pH 7.5, the values of  $q_e$  of both bare-MNPs and PAA-MNPs were equal to 0.003 and 2.135 mol/g, respectively, confirming that the latter can adsorb much larger amounts of  $\text{Ca}^{2+}$  onto its surface than bare MNPs. Therefore, systematic batch experiments were performed to study the adsorption behavior of calcium onto PAA-MNPs changing pH and NaCl concentration. All of the concentrations are expressed in molality (mol/kg) and, for the sake of brevity, we used the symbol  $m$ . Initially, titration experiments were carried using a  $\text{Ca}^{2+}$ -free solution. In these tests, the pH changed between 3 and 8 and NaCl concentration changed between 0.002 and 0.3  $m$ . The results are shown in Figure 6. Here, it is possible to see that as the pH increases the adsorption capacity of the PAA-MNPs decreases, as expected. However, the adsorption decreases also with NaCl concentration at selected pH value. In particular, two types of behaviors can be observed in Figure 6. For NaCl equal to 0.002  $m$ , the adsorption of  $\text{H}^+$  becomes negligible around pH 8. Whereas, for NaCl between 0.1 and 0.3  $m$ , the adsorption of protons is comparable and it becomes negligible around neutral pH.

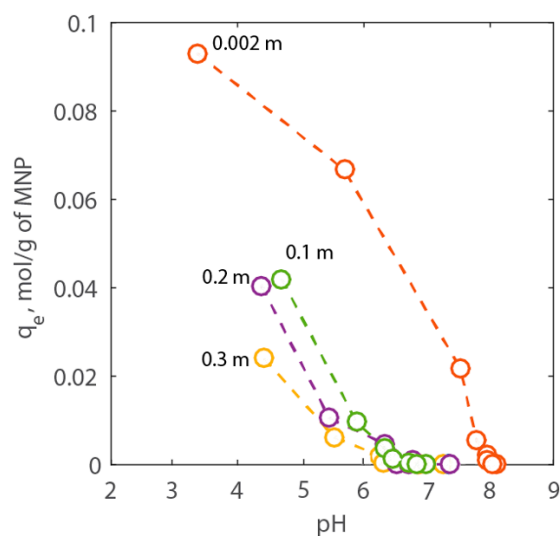


**Figure 6.** Titration results expressed as adsorption capacity of  $\text{H}^+$  vs. pH for NaCl concentration between 0.01 to 3.00 wt % corresponding to 0.002 to 0.3  $m$ , respectively.

To investigate the pH-dependent adsorption of  $\text{Ca}^{2+}$  on PAA-MNPs, tests were performed under various electrolyte concentrations and pH and using a solution with a known initial  $\text{Ca}^{2+}$  concentration. Figure 7 reports the results of the adsorption experiments. Here, it is possible to see that the adsorption of the cation increases with pH but decreases with NaCl concentration. The effect of the electrolyte concentration on adsorption can be ascribed to the decrease of the surface potential ( $\Psi$ ) as NaCl increases and, therefore, the reduction of the intrinsic equilibrium constant of adsorption given in Equations (4) and (5).

The surface complexation model described in Section 3 was used to fit the data shown in Figures 6 and 7 and estimate the parameters. Figure 8 shows the data with the model upon optimization.

The values of the equilibrium constant of the proton adsorption ( $K_1$ ) and the concentration of the reactive sites ( $Z_t$ ) of PAA-MNPs were determined by fitting the titration tests. The estimated average values with their uncertainty are, correspondingly:  $10^{3.16 \pm 1.22}$  kg/mol and  $10^{-3.18 \pm 0.12}$  mol/kg. The estimated value of  $K_1$  is within the uncertainty of the corresponding apparent equilibrium constant of the adsorption of  $H^+$  on phosphino-polycarboxylic acid (PPCA), which is equal to  $10^{4.8 \pm 0.13}$  kg/mol, reported in the literature [30]. The value of the equilibrium constant of calcium adsorption ( $K_2$ ) was determined, maintaining the values of the other parameters (i.e.,  $K_1$  and  $Z_t$ ) within their estimated intervals. The average value of  $K_2$  resulted to be  $10^{2.60 \pm 0.32}$  kg/mol, which is slightly smaller than the corresponding value for the equilibrium constant of the adsorption reaction of calcium onto PPCA, which is  $10^{3.96 \pm 0.46}$  kg/mol, reported in the literature [30].

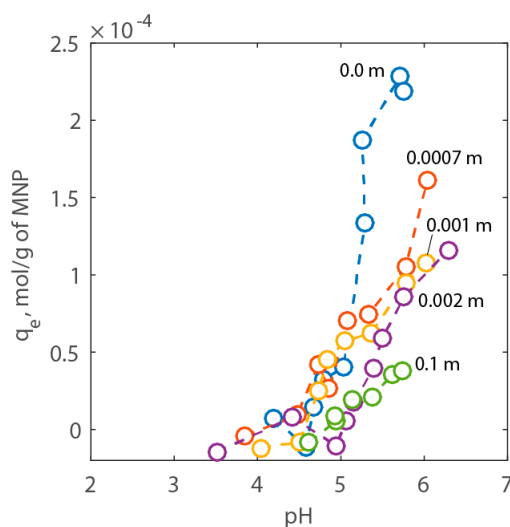


**Figure 7.** Adsorption results expressed as adsorption capacity of  $Ca^{2+}$  vs. pH for NaCl concentration between 0.0 to 1 wt % corresponding to 0.0 to 0.1 m, respectively.

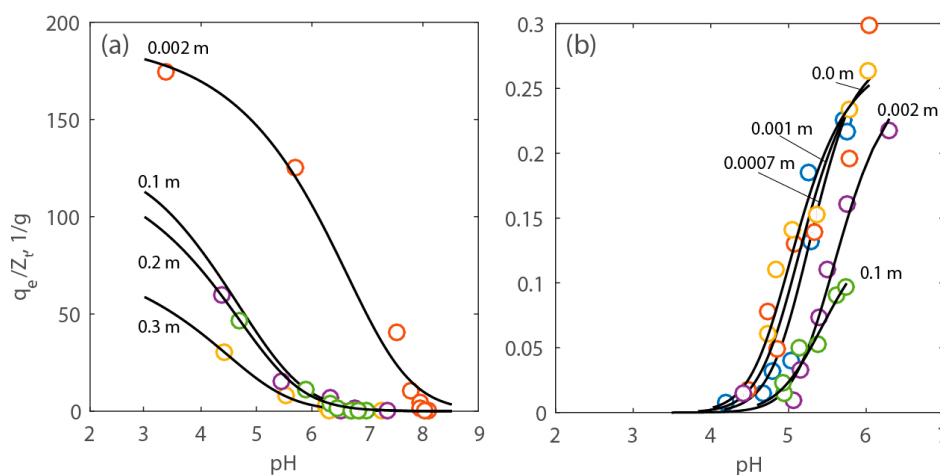


**Figure 8.** Experimental and modeling results expressed as normalized adsorption capacity ( $q_e/Z_t$ ) of  $Ca^{2+}$  vs. pH at various electrolyte concentration. Adsorption capacity of (a) protons and (b) calcium onto PAA-MNPs' surface.

The adsorbed capacity of the PAA-MNPs was normalized by the concentration of estimated total reactive sites,  $Z_t$ , to identify the salt concentration above which adsorption is affected by the presence of the electrolyte without accounting for the effect of surface coating. In Figure 8, it can be seen that, for both calcium and protons, such a critical concentration is approximately 0.1 m. As a matter of fact,

calculations shown in Figure 10 indicate that above this electrolyte concentration there is a significant reduction of the surface potential.

The double layer surface complexation model, which is generally used for the description of adsorption of dissolved species onto mineral surfaces, can capture well the adsorption of a common earth element, such as calcium. The model can describe the competitive adsorption between  $H^+$  and  $Ca^{2+}$  including the effect of electrical surface charge induced by the background electrolyte. To the best of our knowledge, this is the first time that the double layer surface complexation model is used to describe earth element adsorption onto polymer-coated nanoparticles.

Upon adsorption of  $Ca^{2+}$ , nanoparticles agglomerated as it can be observed in Figure 9, which reports images of the PAA-MNPs' suspension at increasing  $Ca^{2+}$  and electrolyte concentration. Measurements of the hydrodynamic diameter of the nanoparticles under these investigated conditions show that at constant calcium concentration,  $D_H$  decreases with the NaCl up to approximately 0.5 m. While, at constant NaCl concentration,  $D_H$  increases with  $Ca^{2+}$  concentration. The latter behavior can be ascribed to the significant decrease of the surface charge, which leads to the reduction of the electrostatic repulsive forces and the increase of the attractive van der Waals forces [31]. As polyacrylic acid chain carries a large number of negative charges, it provides a strong electrostatic repulsion not only between the nanoparticles but also between the intra-chain and inter-chain elements of PAA on the same particle. As calcium is adsorbed, the anionic charges on the PAA attached to the nanoparticles are screened, leading to the compression of highly flexible PAA chains and the consequent decreasing of the repulsive forces and particle distance, hence, allowing the prevalence of the inter-particle van der Waals attraction force and, therefore, favoring aggregation. As shown in our previous works [32,33], nanoparticle agglomeration is beneficial for the overall process of water treatment as it enhances the adsorption by settling induced by a permanent magnet.

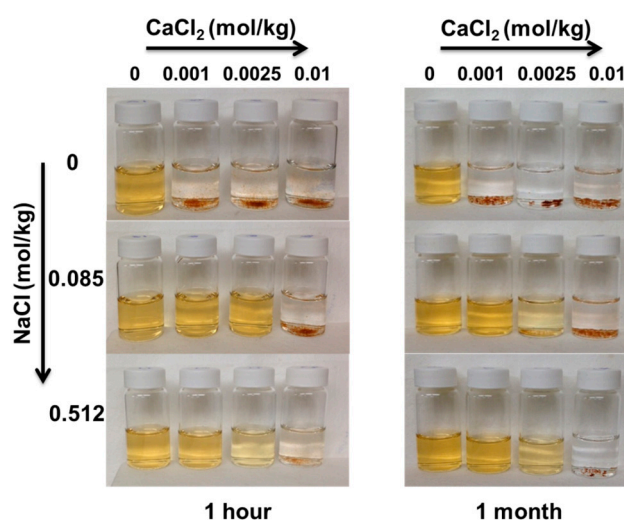


**Figure 9.** Effect of the electrolyte concentration and  $Ca^{2+}$  adsorption on the stability of a PAA-MNPs' suspension of concentration 0.01 g/L.

### 2.3. Simulations

Our results show that the adsorption of  $Ca^{2+}$  becomes important above pH 5. Similar behavior was observed by Hwang et al. [34] for strontium using 5000-dalton PAA at conditions resembling this study. Bartós and Bilewicz [22] investigated the adsorption of alkaline earth elements onto sorbents made by PAA. They report the selectivity of the PAA sorbents as  $Ra^{2+} > Sr^{2+} > Ba^{2+}$ , suggesting that the uptake of  $Ra^{2+}$  is the most significant. However, to the best of our knowledge, the literature does not provide details about the chemical reactions of these cations with PAA and the corresponding equilibrium constants. Therefore, to predict their adsorption, we applied the superimposition of effects,

assuming that above pH 5 the adsorption of each of cation onto PAA-MNPs increases in a similar way. With this assumption, we simulated the adsorption behavior of the major cations in produced water onto PAA-MNPs at various pH values and electrolyte concentrations. We considered the composition of produced water provided by the Marcellus Shale Energy and Environment Laboratory (MSEEL), which resulted with a total concentration of  $\text{Ba}^{2+}$ ,  $\text{Ca}^{2+}$ , and  $\text{Sr}^{2+}$  equal to 0.2 m, a concentration of NaCl of 1 m, and a pH of 6.5 [35]. The concentration of  $\text{Ra}^{2+}$  was not determined. However, from the literature, produced water from wells in the Marcellus Shale might contain on average  $5 \times 10^{-4}$  m of  $\text{Ra}^{2+}$  [36–38].

The results of the simulations expressed as  $q_e$  are shown in Figure 10. For these calculations, model parameters  $K_1$ ,  $K_2$ , and  $Z_t$  were chosen equal to the average estimated values, namely,  $10^4$ ,  $10^3$ , and  $10^{-2}$  mol/kg, respectively. Figure 10 shows a strong effect of pH and electrolyte concentration on the surface potential and, therefore, on surface adsorption. The results indicate that at a given total cation concentration, the maximum adsorption capacity can be achieved within the pH range of the produced water although that maximum declines with electrolyte concentration.

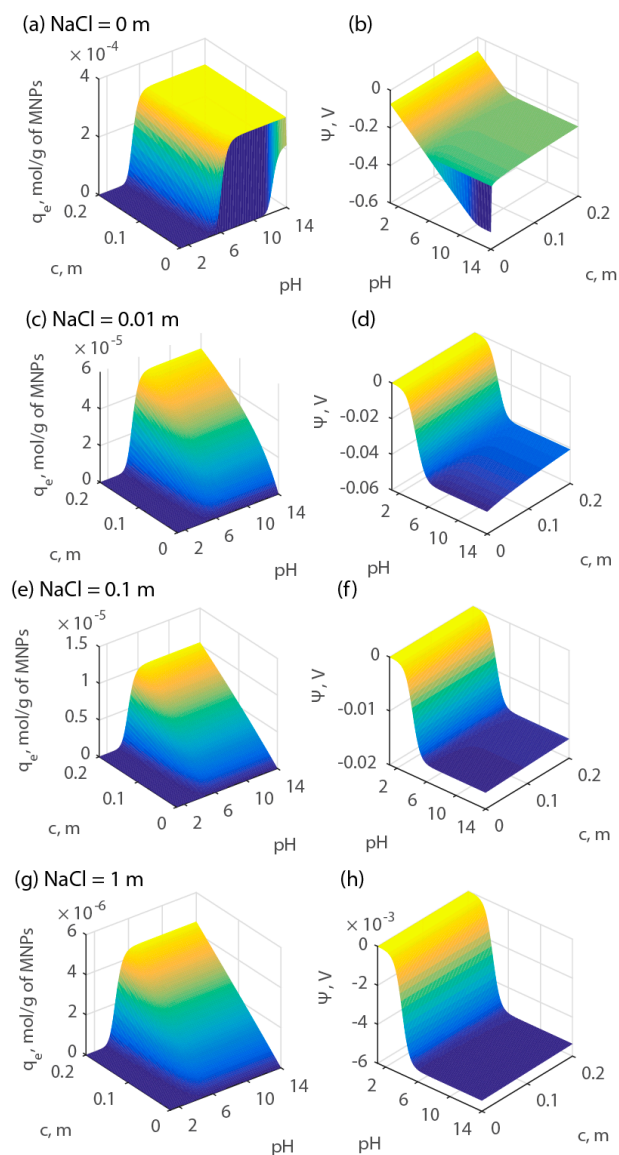


**Figure 10.** Adsorption capacity ( $q_e$ ) and surface potential as a function of pH and cation concentration at various electrolyte concentrations. Parts (a), (c), (e), and (g) report the adsorption capacity of protons. Parts (b), (d), (f), and (h) report the adsorption capacity of calcium.

### 3. Materials and Methods

#### 3.1. Materials

Deionized water (DI-H<sub>2</sub>O) with a resistivity of approximately 18.2 MΩ·cm was obtained from a Barnstead E-pure ultrapure water purification system (Thermo Scientific, Waltham, MA, USA), and used in all experiments. Iron chloride tetrahydrate (FeCl<sub>2</sub>·4H<sub>2</sub>O), iron chloride hexahydrate (FeCl<sub>3</sub>·6H<sub>2</sub>O), and polyacrylic acid (PAA, molecular weight 8000 dalton, 100,000 dalton, and 450,000 dalton) were purchased from Sigma-Aldrich (St. Louis, MO, USA). Sodium chloride (NaCl), sodium hydroxide (NaOH), citric acid monohydrate, ammonium hydroxide, glacial acetic acid, 3-amino propyltriethoxysilane (APTES), 1-ethyl-3-(3-dimethylaminopropyl)carbodiimide (EDC), calcium chloride dihydrate (CaCl<sub>2</sub>·2H<sub>2</sub>O), and hydrochloric acid (HCl) were obtained from Fisher Scientific (Pittsburg, PA, USA). The information about molecular weight of PAA was provided by Sigma-Aldrich. All reagents were used as received without further purification.

#### 3.2. Synthesis of Iron Oxide Magnetic Nanoparticles

Iron oxide magnetic nanoparticles were prepared via a co-precipitation method [23,25,26]. Briefly, an amount of 2.15 g of FeCl<sub>2</sub>·4H<sub>2</sub>O and 5.87 g of FeCl<sub>3</sub>·6H<sub>2</sub>O were dissolved in 100 mL DI-H<sub>2</sub>O, resulting in the molar ratio of Fe<sup>2+</sup> and Fe<sup>3+</sup> at 1:2. Then, an amount of 0.125 g citric acid monohydrate was added to it. After heating the solution up to 90 °C along with vigorous magnetic stirring, 37.5 mL of 20% ammonium hydroxide was loaded to establish alkaline conditions for the initiation of the nucleation of the nanoparticles. Following the continuous reaction for 2 h at 90 °C, the resulting medium was then cooled down to room temperature. The synthesized iron oxide nanoparticles were then washed with DI-H<sub>2</sub>O three times and collected by a permanent magnet of 0.44 T (K&J Magnetics, Inc., Plumsteadville, PA, USA). During each washing step, ultra-sonication was applied to facilitate the dispersion of nanoparticles. Finally, the MNPs were again dispersed in the DI-H<sub>2</sub>O for coating. Particularly, upon the synthesis of the iron oxide magnetic nanoparticles, their coating with polyacrylic acid was accomplished in two steps. First, a coating process was carried out to conjugate the amine group (NH<sub>2</sub>-) on the surface of the iron-oxide magnetic nanoparticles via the covalent bond Fe-O-Si. Second, PAA was used to coat the NH<sub>2</sub>-MNPs by activation of carboxyl acid group with EDC (more details are provided in the next two sections).

#### 3.3. Functionalization of Iron Oxide Magnetic Nanoparticles

Initially, amine functionalization of the iron oxide magnetic nanoparticles was accomplished by a coating method identified as the APTES coating process [23,26]. During this procedure, an amount of 2.96 mL of APTES and 1.34 mL of glacial acetic acid were added into 28 mL of DI-H<sub>2</sub>O at room temperature. After 1 h of hydrolysis at acidic condition, the pH of the solution was adjusted to 8 by adding 2.5 N NaOH. Prior to amine functionalization, 10 mL nanoparticle suspension (50 mg/mL) was sonicated (Branson Digital Sonifier) for 10 min and added dropwise into the hydrolyzed APTES solution. Subsequently, DI-H<sub>2</sub>O was added to reach a total volume of 100 mL. After 24 h of reaction at 65 °C, the suspension was cooled down to room temperature. The amine-functionalized nanoparticles (NH<sub>2</sub>-MNPs) were collected by a magnet, and washed three times with DI-H<sub>2</sub>O. NH<sub>2</sub>-MNPs were then re-suspended in DI-H<sub>2</sub>O, and the pH of the suspension was adjusted to 4.5 by adding HCl (1 N), in order to maintain the stability of nanoparticles.

The modification of the NH<sub>2</sub>-MNPs was performed using PAA with different molecular weights, namely 8000 dalton, 100,000 dalton, and 450,000 dalton. Initially, an amount of 0.2 g of PAA was dissolved into 10 mL H<sub>2</sub>O, and pH was adjusted to 4.7. PAA was then activated by the same molar of EDC at room temperature. After 10 min of EDC activation, 10 mL of NH<sub>2</sub>-MNP suspension (~10 mg/mL) was sonicated and added into the activated PAA solution drop by drop under strong magnetic stirring. At the end, the pH was re-adjusted to 4.7, and the reaction continued for 24 h under the magnetic stirring at room temperature. The different molecular weight of PAA functionalized

NH<sub>2</sub>-MNPs (for the sake of simplicity, they are identified as PAA-8k-MNPs, PAA-100k-MNPs, and PAA-450k-MNPs) were collected by applying the magnetic force, and washed with DI-H<sub>2</sub>O three times. Finally, the produced nanoparticles were re-dispersed in DI-H<sub>2</sub>O and sonicated for 10 min.

### 3.4. Adsorption Experiments

Experiments to investigate the adsorption of protons (hydroxylation) were performed by adding 1 mg of PAA-8k-MNPs into 10 mL of DI-H<sub>2</sub>O with different concentrations of NaCl at room temperature. The initial pH values of all solutions were adjusted between 3.5 and 7.0 by using HCl, NaOH, or a combination of them. After adding the nanoparticles, the solution was sealed into a plastic tube and mixed for 24 h for enough time to achieve the adsorption equilibrium state. The final pH values were measured by a pH probe (Orion, Thermo Scientific, Waltham, MA, USA), and the adsorption isotherms of proton at different salinities were determined. All the experiments were undersaturated with respect to any solid phase at atmospheric conditions.

For the tests, where the adsorption of Ca<sup>2+</sup> was studied together with the effect of the ionic strength, a calcium concentration of 400 ppm ( $1 \times 10^{-2}$  mol/kg) was added to a solution whose pH was adjusted between 3.5 and 7.0. The ionic strength was varied by adding NaCl between 0.0 and 0.5 wt %, i.e., 0.0 and 0.1 mol/kg, correspondingly. Then, a known amount of nanoparticles was added to the solution (approximately 2 mg) and the suspension was allowed to react for 24 h. Finally, the concentration of Ca<sup>2+</sup> was determined by ion chromatography (Dionex ICS-1100, Thermo Scientific, Sunnyvale, CA, USA).

### 3.5. Characterization

#### 3.5.1. Transmission Electron Microscopy

Transmission electron microscopy (TEM, FEI TECNAI G2 F20 X-twin transmission electron microscopy, Hillsboro, OR, USA) measurements were conducted to observe the size and the state of aggregation of the produced particles. For sample preparation, one drop of the diluted nanoparticles, namely an aqueous suspension of 15 µL, was placed on a carbon-coated copper TEM grid, and allowed to be air-dry. TEM images were obtained at the voltage of 80 kV.

#### 3.5.2. Dynamic Light Scattering Analysis

Dynamic light scattering analysis (Malvern Instrument, Malvern, UK) was performed to measure the volume-averaged hydrodynamic diameter ( $D_H$ ) of the produced nanoparticles in DI-H<sub>2</sub>O at room temperature.

#### 3.5.3. Surface Area

Surface area of the PAA-MNPs was quantified using nitrogen sorption on a Quantachrome Instruments NOVA 2000 (Boynton Beach, FL, USA) at 77 K. Brunauer-Emmett-Teller (BET) theory was applied to the adsorption isotherm in the partial pressure region of 0.15–0.3. With this setup, the correlation coefficient was at least 0.995 and the BET constant C was over 20.

#### 3.5.4. Zeta Potential

Zeta potential ( $\zeta$ ) measurements of different MNPs were carried out using the Zetasizer Nano Z (Malvern Instrument, Malvern, UK). Prior to measurements, MNPs were dispersed in a solution containing 0.01 mol/kg of NaCl, and sonicated by an ultra-sonicator for 30 min. The value of the pH of the suspension was adjusted at 7.0.

#### 3.5.5. Thermogravimetric Analysis

Thermogravimetric analysis (TGA, Mettler Toledo TGA/SDTA851e, Columbus, OH, USA) was carried out in order to determine the amount of PAA coating ( $m_c$ ) on the surface of the produced

nanoparticles. The powder sample was heated from 50 °C to 600 °C at a constant rate of 10 °C/min. The weight loss during heating indicated the decomposition of organic components on the surface of MNPs.

### 3.5.6. X-ray Diffraction Analysis

The crystal structure of MNPs was determined by a MSAL-XD2 X-ray diffractometer (XRD), using a Cu-K $\alpha$  radiation ( $\lambda = 0.1541$  nm) as the X-ray source in the  $2\theta$  range of 10°–75°. The measurements were conducted at 30 kV and 30 mA.

### 3.5.7. Magnetization

Saturation magnetization of nanoparticle liquid suspension was measured by a vibrating sample magnetometer (VSM, Microsense model EZ7, Lowell, MA, USA) via a –10 kOe to 10 kOe hysteresis loops using sweep mode at a rate of 250 Oe/s. All of the magnetic fluid samples are measured at 300 K at a DC field with sample vibrating at 75 Hz.

### 3.5.8. MNP Concentration Analysis

Iron concentration in the MNP suspension was measured by inductively-coupled plasma optical emission spectrometry (ICP-OES, Varian, Palo Alto, CA, USA) at the wavelength of 283.2 nm. The nanoparticles were digested by 30 wt % nitric acid, and then the resulting solution was diluted in DI-H<sub>2</sub>O by 10 times for the measurement of iron concentration. The MNP concentration (i.e., magnetite) was calculated by converting from iron concentration.

## 3.6. Adsorption Modeling

The adsorption of calcium onto the functionalized nanoparticles was modeled using surface complexation based on the chemical reactions suggested by Huang and Cheng, Chang, Xiao et al., Stumm et al., and Huang and Stumm [13,21,30,39,40]. Competitive adsorption between H<sup>+</sup> and Ca<sup>2+</sup> was considered with a background electrolyte, i.e., NaCl, where Na<sup>+</sup> behaves as a conservative species. The reactions occur within the diffuse double layer at the solid-liquid interface, with the sorbed ions assigned to the surface layer, while all nonspecifically sorbed counterions assigned to the diffuse double layer. Following Chang [21], the adsorption reactions for H<sup>+</sup> and Ca<sup>2+</sup> onto a reactive PAA surface site, S<sup>−</sup>, are:



The above reactions shown in Equations (2) and (3) are coupled to the hydrolysis reaction of water  $OH^{-} + H^{+} \rightleftharpoons H_2O$  for which the equilibrium constant at 25 °C is  $10^{-14}$ . The associated mass action equations are:

$$K_1 = \frac{\{S-H\}}{a_{H^{+}}\{S^{-}\}} e^{(\Delta ZF\Psi/RT)}, \quad (4)$$

$$K_2 = \frac{\{S_2-Ca\}}{a_{Ca^{2+}}\{S^{-}\}^2} e^{(\Delta ZF\Psi/RT)}, \quad (5)$$

where  $K_1$  and  $K_2$  are the apparent equilibrium constants,  $\{S^{-}\}$  represents the concentration of the PAA reactive site (mol/kg),  $\{S-H\}$  and  $\{S_2-Ca\}$  correspond to the adsorbed concentrations of protons and calcium (mol/kg), respectively,  $a_i$  are the activities of the corresponding subscripts, and the exponential term is the electrostatic or columbic correction factor, with  $F$  is the Faraday constant (96,485 °C/mol),  $\Psi$  is the potential at the surface (V),  $R$  is the gas constant,  $T$  is the temperature (K), and  $\Delta Z$  is the change in charge number of the surface species involved in a surface complexation reaction, equal to +1 in Equation (4) and +2 in Equation (5). The effect of the columbic forces was considered to account for

the effect of the ionic strength, i.e., the concentration of the electrolyte (which includes  $\text{Na}^+$ ), on the competitive adsorption. The site balance equation and the net surface charge density ( $\text{C}/\text{m}^2$ ) are:

$$Z_t = \{S^-\} + \{S\text{-H}\} + 2\{S_2\text{-Ca}\}, \quad (6)$$

$$\sigma = -\left(\frac{F}{AC}\right)\{S^-\}, \quad (7)$$

where  $Z_t$ ,  $A$ , and  $C$  are the total site concentration ( $\text{mol}/\text{kg}$ ), the specific surface area ( $\text{m}^2/\text{g}$ ), and the solid concentration ( $\text{g}/\text{L}$ ), respectively. According to the Gouy-Chapman theory and considering the temperature of  $25\text{ }^\circ\text{C}$ , the net surface charge density,  $\sigma$  is related to the surface potential [41] as:

$$\sigma = 0.1174c^{1/2} \sinh(19.46Z\Psi) \quad (8)$$

where  $c$  is the electrolyte concentration ( $\text{mol}/\text{kg}$ ) and  $Z$  is the valence of the ion in the symmetrical background electrolyte. In our specific case,  $Z$  equals 1, as we used  $\text{Na}^+$  as cation of the background electrolyte. Combining the mass action equations Equations (4)–(8), the adsorption capacity ( $q_e$ ) of PAA-MNPs for  $\text{H}^+$  and  $\text{Ca}^{2+}$  can be derived. Equations (4)–(8) were solved iteratively using the trust-region-reflective algorithm implemented in MATLAB<sup>®</sup> [42] and inverted on adsorption data for calcium to estimate the model parameters.

#### 4. Conclusions

A magnetic nano-adsorbent with iron oxide magnetic nanoparticles as a core and polyacrylic acid as a functional group was successfully synthesized and employed to study the adsorption of  $\text{Ca}^{2+}$  as a congener of alkaline earth elements under various pH and NaCl concentrations. Experimental results show the adsorption of the cation increases with pH, becoming significant around pH 5, and decreases with NaCl concentration. The decrease of the adsorption capacity might be attributed to the compression of the double layer surrounding the nanoparticles with the increase of the electrolyte concentration, which results mathematically in smaller equilibrium constants of adsorption. Qualitative observations of PAA-MNPs' suspensions in various solution composition show that they create large clusters upon  $\text{Ca}^{2+}$  adsorption favoring their magnetic separation. A diffuse double layer surface complexation model accounting for the electrostatic forces was developed to describe the adsorption of  $\text{Ca}^{2+}$  PAA-MNP. The model agrees well with the experimental results and helps to predict the adsorption of the major cations in produced water under various pH and electrolyte concentration. The results indicate that at a given total cation concentration, the maximum adsorption capacity can be achieved within the pH range of the produced water although that maximum declines with electrolyte concentration.

**Acknowledgments:** The authors would like to thank Maersk Oil for the financial and technical supports and Mohsen Ahmadian of Advanced Energy Consortium for performing the VSM measurements. Also the authors would like to thank the Marcellus Shale Energy and Environment Laboratory (MSEEL) to provide the produced water from two gas-extraction wells.

**Author Contributions:** Qing Wang designed and performed the experiments. Valentina Prigiobbe designed the experiments, analyzed the data, developed and validated the model. Chun Huh and Steven L. Bryant advised during the research. Qing Wang and Valentina Prigiobbe wrote the paper.

**Conflicts of Interest:** The authors declare no conflict of interest.

#### References

1. Clark, C.; Veil, J. Produced Water Volumes and Management Practices in the United States. Prepared for U.S. Department of Energy, the National Energy Technology Laboratory; 2009. Available online: <http://www.ipd.anl.gov/anlpubs/2009/07/64622.pdf> (accessed on 21 December 2016).
2. Thiel, G.P.; Lienhard, J.H. Treating produced water from hydraulic fracturing: Composition effects on scale formation and desalination system selection. *Desalination* **2014**, *346*, 54–69. [CrossRef]

3. Lutz, B.D.; Lewis, A.N.; Doyle, M.W. Generation, transport, and disposal of wastewater associated with Marcellus shale gas development. *Water Resour. Res.* **2013**, *9*, 647–656. [[CrossRef](#)]
4. Groundwater Protection Council (GWPC). Modern Shale Gas Development in the United States: A Primer. Available online: <https://energy.gov/fe/downloads/modern-shale-gas-development-united-states-primer> (accessed on 9 February 2017).
5. Shaffer, D.L.; Arias Chavez, L.H.; Ben-Sasson, M.; Castrillin, S.R.-V.; Yip, N.Y.; Elimelech, M. Desalination and reuse of high-salinity shale gas produced water: Drivers, technologies, and future directions. *Environ. Sci. Technol.* **2013**, *47*, 9569–9583. [[CrossRef](#)] [[PubMed](#)]
6. Ge, F.; Li, M.-M.; Ye, H.; Zhao, B.-X. Effective removal of heavy metal ions  $\text{Cd}^{2+}$ ,  $\text{Zn}^{2+}$ ,  $\text{Pb}^{2+}$ ,  $\text{Cu}^{2+}$  from aqueous solution by polymer-modified magnetic nanoparticles. *J. Hazard. Mater.* **2012**, *211*, 366–372. [[CrossRef](#)] [[PubMed](#)]
7. Liu, Y.; Chen, M.; Yongmei, H. Study on the adsorption of Cu (II) by EDTA functionalized  $\text{Fe}_3\text{O}_4$  magnetic nano-particles. *Chem. Eng. J.* **2013**, *218*, 46–54. [[CrossRef](#)]
8. Takafuji, M.; Ide, S.; Ihara, H.; Xu, Z. Preparation of poly (1-vinylimidazole)-grafted magnetic nanoparticles and their application for removal of metal ions. *Chem. Mater.* **2004**, *16*, 1977–1983. [[CrossRef](#)]
9. Zhang, J.; Zhai, S.; Li, S.; Xiao, Z.; Song, Y.; An, Q.; Tian, G. Pb(II) removal of  $\text{Fe}_3\text{O}_4$  with  $\text{SiO}_2\text{-NH}_2$  core-shell nanomaterials prepared via a controllable sol-gel process. *Chem. Eng. J.* **2013**, *215*, 461–471. [[CrossRef](#)]
10. Ko, S.; Prigiobbe, V.; Huh, C.; Bryant, S.L.; Bennetzen, M.V.; Mogensen, K. Accelerated oil droplet separation from produced water using magnetic nanoparticles. In Proceedings of the SPE Annual Technical Conference and Exhibition, Amsterdam, The Netherlands, 27–29 October 2014.
11. Ling, M.M.; Wang, K.Y.; Chung, T.-S. Highly water-soluble magnetic nanoparticles as novel draw solutes in forward osmosis for water reuse. *Ind. Eng. Chem. Res.* **2010**, *49*, 5869–5876. [[CrossRef](#)]
12. Wang, Q.; Prigiobbe, V.; Huh, C.; Bryant, S.L.; Mogensen, K.; Bennetzen, M.V. Removal of divalent cations from brine using selective adsorption onto magnetic nanoparticles. In Proceedings of the International Petroleum Technology Conference, Kuala Lumpur, Malaysia, 10–12 December 2014.
13. Huang, S.-H.; Chen, D.-H. Rapid removal of heavy metal cations and anions from aqueous solutions by an amino-functionalized magnetic nano-adsorbent. *J. Hazard. Mater.* **2009**, *163*, 174–179. [[CrossRef](#)] [[PubMed](#)]
14. Sud, D.; Mahajan, G.; Kaur, M. Agricultural waste material as potential adsorbent for sequestering heavy metal ions from aqueous solutions—A review. *Bioresour. Technol.* **2008**, *99*, 6017–6027. [[CrossRef](#)] [[PubMed](#)]
15. Xu, Y.; Zhuang, L.; Lin, H.; Shen, H.; Li, J.W. Preparation and characterization of polyacrylic acid coated magnetite nanoparticles functionalized with amino acids. *Thin Solid Films* **2013**, *544*, 368–373. [[CrossRef](#)]
16. Pan, B.; Pan, B.; Zhang, W.; Lv, L.; Zhang, Q.; Zheng, S. Development of polymeric and polymer-based hybrid adsorbents for pollutants removal from waters. *Chem. Eng. J.* **2009**, *151*, 19–29. [[CrossRef](#)]
17. Mahdavian, A.R.; Mirrahimi, M.A.-S. Efficient separation of heavy metal cations by anchoring polyacrylic acid on superparamagnetic magnetite nanoparticles through surface modification. *Chem. Eng. J.* **2010**, *159*, 264–271. [[CrossRef](#)]
18. Morales, D.V.; Rivas, B.L. Poly (2-acrylamidoglycolic acid-co-2-acrylamide-2-methyl-1-propane sulfonic acid) and poly (2-acrylamidoglycolic acid-co-4-styrene sodium sulfonate): Synthesis, characterization, and properties for use in the removal of Cd (II), Hg (II), Zn (II), and Pb (II). *Polym. Bull.* **2015**, *72*, 339–352.
19. Moulay, S.; Bensacia, N. Removal of heavy metals by homolytically functionalized poly (acrylic acid) with hydroquinone. *Int. J. Ind. Chem.* **2016**, *7*, 369–389. [[CrossRef](#)]
20. Sezgin, N.; Balkaya, N. Adsorption of heavy metals from industrial wastewater by using polyacrylic acid hydrogel. *Desalination Water Treat.* **2016**, *57*, 2466–2480. [[CrossRef](#)]
21. Chang, D.M. The binding of free calcium ions in aqueous solution using chelating agents, phosphates and poly (acrylic acid). *J. Am. Oil Chem. Soc.* **1983**, *60*, 618–622. [[CrossRef](#)]
22. Bartós, B.; Bilewicz, A. Effect of crown ethers on  $\text{Sr}^{2+}$ ,  $\text{Ba}^{2+}$ , and  $\text{Ra}^{2+}$  uptake by tunnel-structure ion exchangers. *Solvent Extr. Ion Exch.* **2006**, *24*, 261–269. [[CrossRef](#)]
23. Bagaria, H.G.; Xue, Z.; Neilson, B.M.; Worthen, A.J.; Yoon, K.Y.; Nayak, S.; Cheng, V.; Lee, J.H.; Bielawski, C.W.; Johnston, K.P. Iron oxide nanoparticles grafted with sulfonated copolymers are stable in concentrated brine at elevated temperatures and weakly adsorb on silica. *ACS Appl. Mater. Interfaces* **2013**, *5*, 3329–3339. [[CrossRef](#)] [[PubMed](#)]
24. Bee, A.; Massart, R.; Neveu, S. Synthesis of very fine maghemite particles. *J. Magn. Magn. Mater.* **1995**, *149*, 6–9. [[CrossRef](#)]

25. Massart, R. Preparation of aqueous magnetic liquids in alkaline and acidic media. *IEEE Trans. Magn.* **1981**, *17*, 1247–1248. [[CrossRef](#)]
26. Xue, Z.; Foster, E.; Wang, Y.; Nayak, S.; Cheng, V.; Ngo, V.W.; Pennell, K.D.; Bielawski, C.W.; Johnston, K.P. Effect of grafted copolymer composition on iron oxide nanoparticle stability and transport in porous media at high salinity. *Energy Fuels* **2014**, *28*, 3655–3665. [[CrossRef](#)]
27. Yoon, K.Y.; Li, Z.; Neilson, B.M.; Lee, W.; Huh, C.; Bryant, S.L.; Bielawski, C.W.; Johnston, K.P. Effect of adsorbed amphiphilic copolymers on the interfacial activity of superparamagnetic nanoclusters and the emulsification of oil in water. *Macromolecules* **2012**, *45*, 5157–5166. [[CrossRef](#)]
28. Takafuji, M.; Kitaura, K.; Nishiyama, T.; Govindarajan, S.; Gopal, V.; Imamura, T.; Ihara, H. Chemically tunable cationic polymer-bonded magnetic nanoparticles for gene magnetofection. *J. Mater. Chem. B* **2014**, *2*, 644–650. [[CrossRef](#)]
29. Ortega, D. *Magnetic Nanoparticles: From Fabrication of Clinical Application*, 1st ed.; CRC Press: Hoboken, NJ, USA, 2012.
30. Xiao, J.; Kan, A.T.; Tomson, M.B. Acid–base and metal complexation chemistry of phosphino-polycarboxylic acid under high ionic strength and high temperature. *Langmuir* **2001**, *17*, 4661–4667. [[CrossRef](#)]
31. Phenrat, T.; Saleh, N.; Sirk, K.; Tilton, R.D.; Lowry, G.V. Aggregation and sedimentation of aqueous nanoscale zerovalent iron dispersions. *Environ. Sci. Technol.* **2007**, *41*, 284–290. [[CrossRef](#)] [[PubMed](#)]
32. Prigiobbe, V.; Ko, S.; Huh, C.; Bryant, S.L. Measuring and modeling the magnetic settling of superparamagnetic nanoparticle dispersions. *J. Colloid Interface Sci.* **2015**, *447*, 58–67. [[CrossRef](#)] [[PubMed](#)]
33. Prigiobbe, V.; Ko, S.; Wang, Q.; Huh, C.; Bryant, S.L.; Bennetzen, M.V. Magnetic nanoparticles for efficient removal of oilfield “contaminants”: Modeling of magnetic separation and validation. In Proceedings of the SPE International Symposium on Oilfield Chemistry, The Woodlands, TX, USA, 13–15 April 2015.
34. Hwang, E.-D.; Lee, K.-W.; Choo, K.-H.; Choi, S.-J.; Kim, S.-H.; Yoon, C.-H.; Lee, C.-H. Effect of precipitation and complexation on nano-filtration of strontium-containing nuclear wastewater. *Desalination* **2002**, *47*, 289–294. [[CrossRef](#)]
35. Zi, Y.; Prigiobbe, V. Effect of salinity and temperature on pH-dependent transport of heavy metals and radionuclides in reactive porous media. **2017**. in preparation.
36. He, C.; Li, M.; Liu, W.; Barbot, E.; Vidic, R.D. Kinetics and equilibrium of barium and strontium sulfate formation in Marcellus Shale flowback. *Water J. Environ. Eng.* **2014**, *140*, B4014001. [[CrossRef](#)]
37. Ferrar, K.J.; Michanowicz, D.R.; Christen, C.L.; Mulcahy, N.; Malone, S.L.; Sharma, R.K. Assessment of effluent contaminants from three facilities discharging Marcellus Shale wastewater to surface waters in Pennsylvania. *Environ. Sci. Technol.* **2013**, *47*, 3472–3481. [[CrossRef](#)] [[PubMed](#)]
38. Warner, N.R.; Christie, C.A.; Jackson, R.B.; Vengosh, A. Impacts of shale gas wastewater disposal on water quality in western Pennsylvania. *Environ. Sci. Technol.* **2013**, *47*, 11849–11857. [[CrossRef](#)] [[PubMed](#)]
39. Stumm, W.; Huang, C.P.; Jenkins, S.R. Specific Chemical Interactions Affecting the Stability of Dispersed Systems. *Croat. Chem. Acta* **1970**, *42*, 223–245.
40. Huang, C.-P.; Stumm, W. Specific adsorption of cations on hydrous  $\gamma$ -Al<sub>2</sub>O<sub>3</sub>. *J. Colloid Interface Sci.* **1970**, *43*, 409–420. [[CrossRef](#)]
41. Dzombak, D.A.; Morel, F.M.M. *Surface Complexation Modeling: Hydrous Ferric Oxide*; Wiley: New York, NY, USA, 1990.
42. *MATLAB Version 8.6.0*; The MathWorks Inc.: Natick, MA, USA, 2015.

